BEST AVAILABLE IMAGES

Defective images within this document are accurate representations of the original documents submitted by the applicant.

Defects in the images may include (but are not limited to):

- BLACK BORDERS
- TEXT CUT OFF AT TOP, BOTTOM OR SIDES
- FADED TEXT
- ILLEGIBLE TEXT
- SKEWED/SLANTED IMAGES
- COLORED PHOTOS
- BLACK OR VERY BLACK AND WHITE DARK PHOTOS
- GRAY SCALE DOCUMENTS

IMAGES ARE BEST AVAILABLE COPY.

As rescanning documents *will not* correct images, please do not report the images to the Image Problem Mailbox.

APPENDIX A

M. Misawa, I. Tiseanu, H.-M. Prasser, N. Ichikawa, M. Akai

Ultra-fast x-ray tomography for multi-phase flow interface dynamic studies

The present paper describes the concept of a fast scanning X-ray tomograph, the hardware development, and measurement results of gas-liquid two-phase flow in a vertical pipe. The device uses 18 pulsed X-ray sources activated in a successive order. In this way, a complete set of 18 independent projections of the object is obtained within 38 ms, i. e. the measuring rate is about 250 frames per second. Finally, to evaluate the measurement capability of the fast X-ray CT, a wire-mesh sensor was installed in the flow loop and both systems were operated for the same two-phase flow simultaneously. Comparison of the time series of the cross section averaged void fraction from both systems showed sufficient agreement for slug flow at large void fractions, while the fast CT underestimated the void fraction of bubbly flow especially in low void fraction range. For the wire-mesh sensor, coerced deformation of slug bubble interface was found. Further hardware improvement is in progress to achieve better resolution with the fast X-ray CT scanner.

Ultra-schnelle Röntgentomographie für das Studium der Dynamik von Phasengrenzflächen in Mehrphasenströmungen. *Der Beitrag beschreibt das Konzept eines schnellen Röntgentomographen, die Hardwareentwicklung und Messergebnisse aus einer Zweiphasenströmung eines Flüssigkeits-Gas-Gemischs in einer vertikalen Rohrleitung. Das Gerät verfügt über 18 gepulste Röntgenquellen, die in schneller Folge aktiviert werden. Auf diese Weise wird ein vollständiger Satz aus 18 Projektionen des Objekts innerhalb von 38 ms gewonnen. Die Messfrequenz beträgt demzufolge ca. 250 Bilder pro Sekunde. Um das System zu testen, wurde ein Gittersensor in die Strömungsschleife eingebaut. Beide Geräte wurden gemeinsam zur Aufnahme der gleichen Zweiphasenströmung genutzt. Der Vergleich des Zeitverlaufs des querschnittsgemittelten Gasgehalts zeigt eine gute Übereinstimmung zwischen beiden Verfahren im Gebiet der Pfropfenströmung. Bei einer Blasenströmung kommt es zu einer Unterbewertung des Gasgehalts durch den Röntgentomographen. In Bezug auf den Gittersensor wurde eine Deformation der Großblasen gefunden. Zukünftige Hardware-Verbesserungen zur Erhöhung der Auflösung des Röntgentomographen sind geplant.*

1 Introduction

Use of X-ray CT (Computer Tomography) system has been extended from medical fields to a variety of industrial applications [1, 2]. Among them is the visualization of multi-dimensional void distribution of two-phase flow in tubes. Mitsutake et al. [3] and Morooka et al. [4] used medical X-ray CT scanners modified for void fraction measurement within rod bundles. The results were comparable with their predictions based on three-fluid model. Recently Tiseanu et al. applied cone beam tomography to bubbly flow in a vertical pipe and obtained sharper void peaks near the wall than previously reported [5]. Cone beam tomography is a 3D visualization technique and allowed them to collect multi-slice data in vertical direction within the same amount of scanning time as 2D systems. Gamma-ray is another form of generating high energy photons. Kumar et al. built a tomography system based on Cs-137 gamma ray source for void distribution measurement of a bubble column [6]. Although gamma ray sources eliminate the beam-hardening effect, low photon flux results in long scanning time. However, these systems are not applicable to dynamic interface detection of multi-phase flow because of low time resolution compared to transition time of interfaces. To visualize dynamic interfaces in multi-phase flow, time-resolved X-ray CT scanners have been developed by Hori and Akai [7], Hori et al. [8], and Misawa et al. [9] (Fig. 1). Scanning time of these systems is reduced by an order of two compared to existing ones. In pursuit of time resolution, however, spatial resolution is sacrificed due to less numbers of detector elements and views. The present paper describes the concept of fast scanning capability, hardware development, and measurement results of gas-liquid two-phase flow in a vertical pipe. Finally, to evaluate the measurement capability of the fast X-ray CT, the wire-mesh sensor [10]

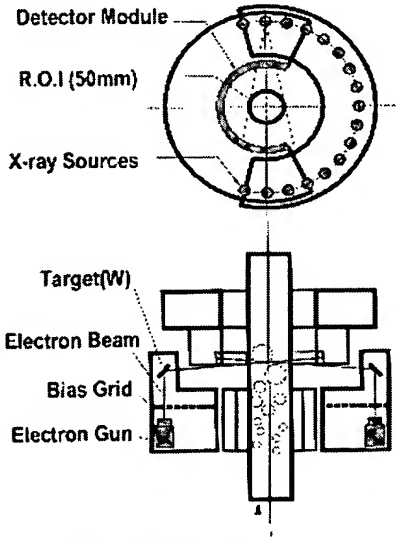

Fig. 1. Design of the fast X-ray CT

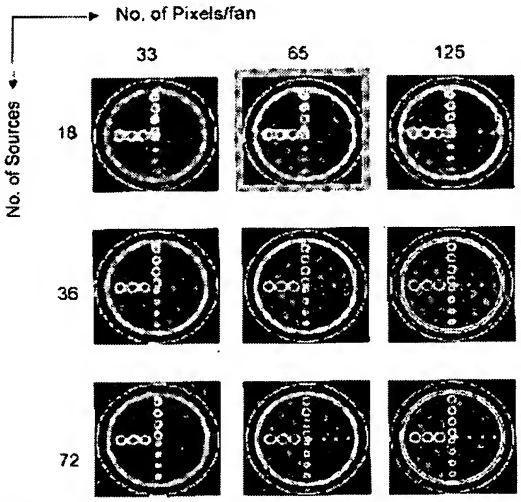

Fig. 2. Simulation of a cylinder phantom cross section with different numbers of detector elements and X-ray sources

was installed in the flow loop and both systems were operated for the same two-phase flow simultaneously. The results showed that the time series of cross section averaged void fraction agreed to each other for slug flow at large void fraction, but that the wire-mesh sensor was suitable for bubbly flow at low void fraction. From the comparison of the time series data, coerced deformation of slug bubble interface was suggested for the wire-mesh sensor.

2 Selection of parameters based on simulation

The requirements set for the multi-phase flow measurement were 1) spatial resolution <3.0 mm, 2) time resolution <4 msec. per scan, and 3) measurement area diameter <50 mm. Before hardware construction, numerical simulations were conducted to see whether the above requirements were achieved. Cylindrical and spherical plastic phantoms as well as their combination were numerically modeled and their projection data was calculated based on the X-ray energy, attenuation coefficient of the materials, distance between the X-ray sources and detectors. Among several key parameters, the number of X-ray sources and detector pixels are most important parameters which determines uniquely the spatial resolution in the reconstructed image. Fig. 2 shows the reconstructed images of a cylindrical rod with several vertical holes of different diameters. Spatial resolution varies by changing the number of sources and the number of detector pixels. In fact, current system consists of 18 X-ray sources and 60 pixels per fan beam, which theoretically allows us to observe 2 mm diameter holes under a situation free of noise and misalignment. One can see that an increase in the X-ray sources are more efficient to improving the resolution than that in the pixels in this design. However, as the X-ray sources increases, the time resolution and intensity will suffer because relatively large diameter of the X-ray tubes results in long distance between X-ray sources and detectors.

3 Hardware elements of the fast X-ray CT

3.1 System outline

To complete a single scan on the order of milliseconds, the mechanical scanning motion should be avoided. Instead, the 18 X-ray sources are placed along a circle of radius 120.5 mm from the center of measurement region, and emission of X-ray is controlled by electrical switching. Fig. 3 illustrates the switching mechanism of the X-ray tubes. Electrons keep emitted from the heated filament of electron guns but allowed to pass through the bias grid aperture only when the negative bias was removed. After passing through the grid aperture, the electrons are accelerated in the 40–160 kV electric field and hit the tungsten target embedded in the common anode ring. The X-ray fan beam spreads over 24 degrees and activates 60 pixels on the detector. High voltage is continuously applied on the anode ring from the voltage source outside the vacuum chamber. All x-ray sources without glass tubes are installed in the vacuum chamber. This configuration was adopted to reduce the pitch of X-ray focuses for increasing spatial resolution. To avoid the interaction of X-ray beams with the detector, X-ray focus plane is offset from the detector plane by 10–20 mm. This allows for photons to transmit through the object and reach the detector elements on the opposite side of the X-ray source at an elevated angle. From the point of image reconstruction, data collection along a path elevated from the horizontal plane can be a cause of artifact. However, simulation result showed that the effect is not significant if the elevation angle is less than 15 degree. Emission of X-ray and data acquisition is synchronized by a pulse controller. Following a start trigger, the bias grids are sequentially disarmed for 100 microseconds and all the detector elements are scanned upon each X-ray emission. During the next 100 microseconds, the X-ray sources rest and the data is transferred to the computer. After the 18th X-ray emission is done, another data acquisition is made without X-rays. This serves as a offset level for the data sequence in a single scan. From a total of 19 data set thus acquired at different angles, a cross section image is reconstructed. Table 1 lists the main design parameters of the fast X-ray CT scanner. With the given parameters, a spatial resolution of 2.6 mm and the scanning rate of 263 Hz can be attained. Image reconstruction, base on a filtered back projection, is carried out on off-line after all the data is stored in a tiff-type format. The filtered back projection method is used for 2D image reconstruction in 101×101 pixel format over a 50 mm diameter region of in-

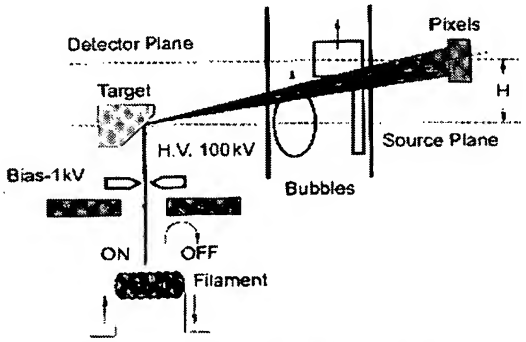

Fig. 3. Switching mechanism of multiple pulsed X-ray sources

Table 1. Fast X-ray CT specifications

Number of X-ray sources	18
Acceleration voltage	160 kV max.
Beam current	10 mA max.
Scan time per slice	3.8 msec
Scan rate	263 slices
Beam thickness	5 mm
Number of detectors	256
Detector device	CdTe
No. of detectors/fan beam	60
Maximum object diameter	50 mm
Designed spatial resolution	2.6 mm
Fan beam angle	24 degrees
X-ray source ring diameter	241 mm
Detector ring diameter	163.4 mm
A/D resolution	12 bit
Integration time	0.2 msec. min.
Image reconstruction	FBP
Filter Type	Shepp-Logan

terest. A reference scale of 50 mm was digitized into 101 pixels, converting to 0.495 mm in length or 0.245 mm^2 in area per pixel.

3.2 Development of a high efficiency semi-conductor detector

How to collect a sufficient amount of photons in the detector during the short period of pulsed X-ray irradiation is the key issue of detector design. Semi-conductor solid detectors convert incident photon energy to carrier signals directly inside the crystal, resulting in higher conversion efficiency than scintillator detectors by an order (Fig. 4). Cadmium Telluride (CdTe) crystal was selected as the detector material because of its large atomic number and large band gap. For the X-ray energy around 100 kV, more than 95 % photons are captured by a 1.0 mm thick crystal. The band gap of CdTe crystal is 1.44eV, and this allows us to use the device without cooling. On the surfaces of a substrate of CdTe monocrystal (size: 5×20×1 mm), anode and cathode pixel patterns are printed by photolithography technique. The effective pixel size is 0.3×0.8 mm with a pitch of 1.425 mm. A set of 32 pixels is allocated in a single detector module. Signal processing of this charge-sensitive device is made by a 32 channel CMOS IC. The chip is placed close to the sensing crystal to reduce the noise effect. The developed detector consists of 8 modules having 32 pixels each and completes scanning over 256 pixels in 200 micro seconds. After a successful radiography tests, the detector modules were assembled into the fast CT scanner.

4 Dynamic interface measurement

4.1 Examination of data quality

Prior to fluid experiment, measurement capability of the cross-section and the interface was evaluated by scanning plastic phantoms with know dimensions. In the first series of experiment, spheres and cylinders of different sizes moved through the measuring plane and their volumes and surface areas were compared with true values by setting a threshold value based on intensity histogram. The results indicate that the volumes and interfaces for velocities less than 1.0m/s can be reproduced within 20 % of measurement accuracy.

Next, a slug unit phantom was made to simulate more realistic situation. The phantom has a semi-spherical dome, a cylindrical part of 2 mm wall thickness, and cylindrical and spherical voids of 3–6 mm in diameter. The reconstructed images of several cross sections for the moving velocity of 0.3 m/s are shown in Fig. 5. When the dome passes through the measuring plane, its boundary looks diffused because the

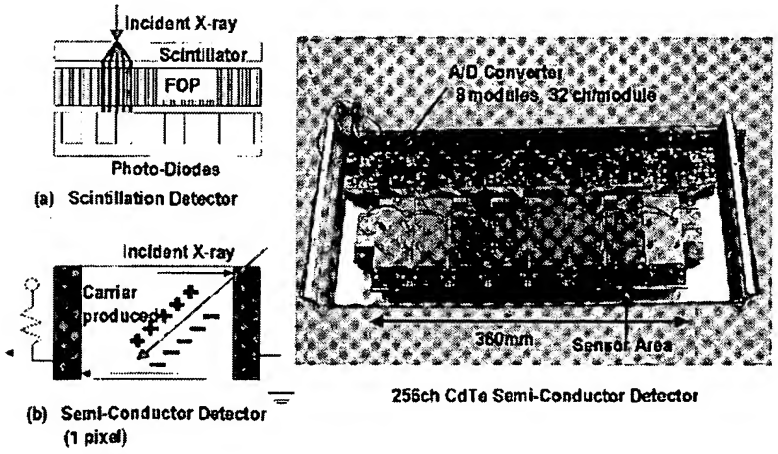

Fig. 4. A high efficiency semi-conductor X-ray detector assembly for the fast X-ray CT scanner

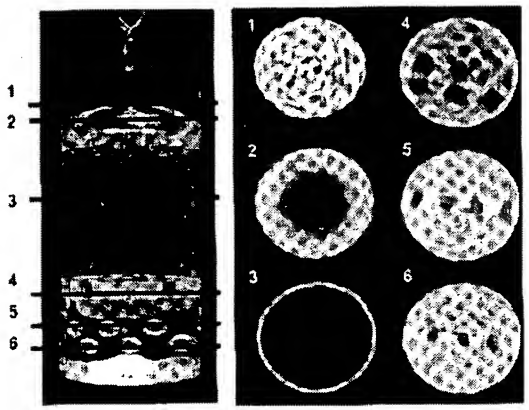

Fig. 5. Reconstructed images of a slug shape phantom

cross section shape was constantly changing in the axial direction while being scanned. On contrary, the cylindrical part was reproduced clearly since the cross section shape remained the same during the scanning period. Cylindrical and spherical cavities of 3–6 mm in diameter were also reproduced successfully.

Fig. 6 shows the average intensity profiles of reconstructed images for water alone in a 42 mm diameter pipe and for bubbles in the water. Air was introduced through a 4 mm diameter nozzle placed at the bottom of the pipe. The average intensity fluctuation for water is considered to be measurement noise. When a signal falls below this level, identification of individual bubbles becomes difficult. However, from the fact that the noise signal fluctuates around level zero, the average void fraction over the cross section can be measured from level zero with an error on the order of noise fluctuation.

4.2 Air-water two-phase flow

With the knowledge of signal characteristics in measurement, the superficial gas velocity was increased from 0.013 to 0.091 m/s. For visualization of interface, the attenuation coefficient matrix is mapped to in the 256 grayscale level. A threshold level was chosen by referring to histograms for each condition. The figures shown in Fig. 7 represent the time series of spatial void distribution at the measuring plane. Reconstructed images in 101 × 101 pixel format are stacked in order with a slice thickness of one pixel. In reality, however, the local interface velocity are changing in time. The best approximation available is to use the average bubble velocity after calculating the average void fraction. The overall distribution patterns are sufficiently reserved regardless of instantaneous fluctuation of interfaces.

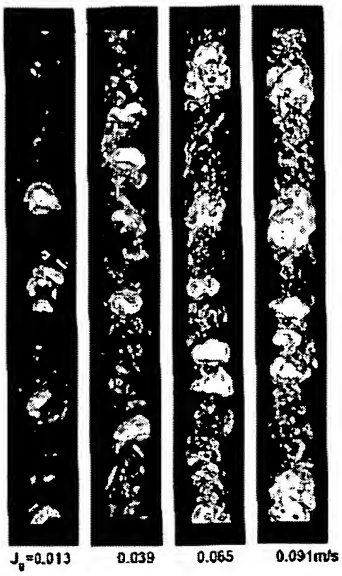

Fig. 7. Slug bubbles in a 42mm diameter vertical pipe (j_f = 0.0 m/s)

In addition to slug flow, bubbly flow was created by introducing air through a porous metal with its pore size of 100 micro meter. Although the individual bubble shape is difficult to recognize, the concentration of void in the cross section is visualized. The image shows the concentration of bubbles near the pipe wall for concurrent flow under relatively low gas flow rates. As the gas flow rate increases, bubble concentration starts to occur in the central region of the pipe.

4.3 Evaluation of data

The measured void distribution in the cross section contains information on the void fraction and the interface area con-

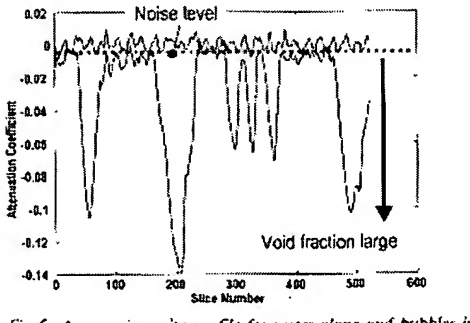

Fig. 6. Average intensity profile for water alone and bubbles in water (j_g = 0.091 m/s)

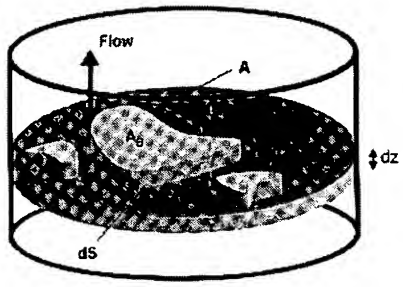

Fig. 8. A slice "disk" of two-phase flow extracted by the fast X-ray CT

centration, both of which are essential quantities in multi-dimensional two-phase flow analysis. After image reconstruction, a slice disk including 2D bubble distribution is obtained (Fig. 8). Assuming that the void distribution is steady in time and the slice thickness is sufficiently thin, the void fraction is the ratio of the total bubble cross section area Sum(A_{Bi}) to the total flow area A_0:

$$\alpha = \Sigma(A_{Bi})/A_0 \quad (1)$$

On the other hand, the interfacial area concentration is by definition the amount of interface in a unit volume. The amount of interface is calculated as the product of the bubble boundary and the thickness of the disk. Thus,

$$a_i = \Sigma(L_{Bi})d\alpha/A_0 d\alpha = \Sigma(L_{Bi})/A_0 \quad (2)$$

Since the total flow area remain unchanged, both quantities depend on the cross section and perimeter of the bubbles in the slice disk.

5 Comparison with the wire-mesh sensor

Advantages of the fast X-ray CT are its non-invasiveness and applicability to all types of multi-phase flow including solids. Wire-mesh sensor is especially useful when an on-line monitoring is necessary and the flow velocity is relatively large. However, it is difficult to calibrate the measured data each alone since the absolute values are often unknown in actual two-phase flow. When both systems are applied to the same two-phase flow, it is curious to see how much the instantaneous values differ from each other. Both methods were applied to the same air-water two-phase flow to validate their measurements as well as to clarify the difference.

5.1 Experimental setup

The 16×16 wire-mesh sensor and the fast X-ray CT scanner were applied simultaneously to the two-phase flow in a 42 mm diameter vertical pipe. A part of the apparatus is shown in Fig. 9. Since the fast X-ray CT is non-invasive, its measurement plane was set at 15 mm upstream of that of the wire-mesh sensor. This interval was the minimum to avoid interference of each other's measurement. The measuring plane was located 1.19 m from the air-water mixing chamber. The starting trigger was shared by the both systems and the data for 4.0 s were recorded under various flow conditions. Sampling frequency for the wire-mesh sensor and the fast X-ray CT were set at 1053 Hz and 263 Hz, respectively. The total cross section images for the wire-mesh sensor was 4211, while the fast X-ray CT recorded

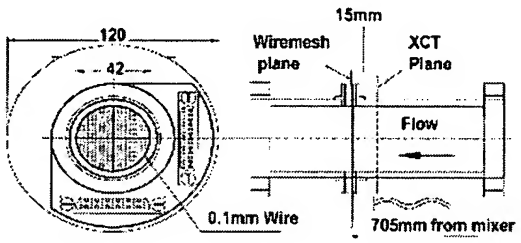

Fig. 9. Wire-mesh sensor and the fast X-ray CT measurement planes

1052 slices. The superficial gas velocity ranged from 0.02 to 0.40 m/s, while the liquid velocity varied from 0.0–0.69 m/s. Both bubbly and slug flow patterns were tested under the same flow conditions.

5.2 Results of void fraction measurement

With the wire-mesh sensor and the fast X-ray CT, large slug bubbles were similarly reproduced, except that the interface shape appears to be elongated for the wire-mesh measurement. This is caused either by the interface repulsion against the sensor wires or formation of liquid bridges between the sensor wires. High-speed video observation during the wire-mesh measurement also indicated such cases may occur. On the other hand, the fast CT measurement provided relatively small values for the void fraction component in the liquid hold up. This difference comes from the sensitivity of the measurement system toward small bubbles. As the invasive method, the wire-mesh sensor directly senses the existence of small bubbles, while the X-ray contrast becomes smaller as the bubble size is reduced. In processing of the fast X-ray CT data, a constant threshold level was used to make binary images for void fraction count. Use of variable thresholds depending on the bubble size will improve the measurement.

Time series data of the cross section averaged void fraction were compared for the both measurements. The wire-mesh data was re-sampled at 263 Hz to match the sampling frequency of the fast CT. Then the average time lag was obtained by calculating the cross correlation of the profiles. Fig. 10 shows the void fraction time series after re-sampled and adjusted by the time lag. Again the slug bubble profiles are similar to each other, except the front-edge deformation as seen in the reconstructed image. Histograms of the void fraction values for both measurements indicates their difference clearly. Although the overall shape resembles, the peak

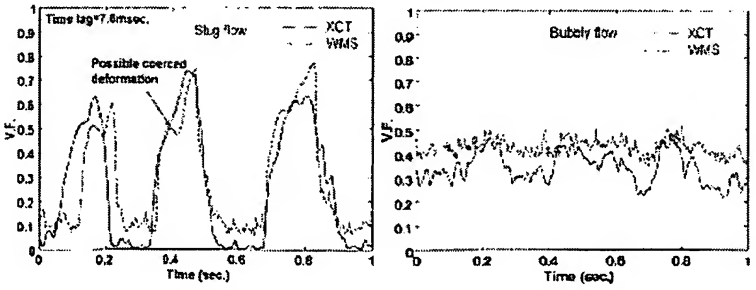

Fig. 10. Time series of the cross section averaged void fraction obtained by the wire-mesh sensor and the fast X-ray CT (j_g = 0.4 m/s, j_l = 0.0 m/s)

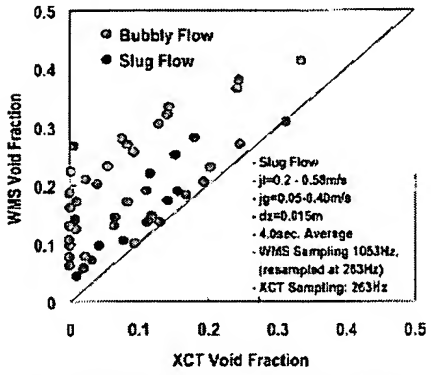

Fig. 11. Comparison of cross section average void fraction measured by the wire-mesh sensor and the fast X-ray CT

of the wire-mesh measurement near void fraction 0.5 may be caused by false peak due to coerced deformation of slug bubbles. On the other hand, the large peak near void fraction zero in the fast X-ray CT measurement indicates its inability to detect small bubbles which the wire-mesh sensor successfully captured. Regarding bubbly flow, both measurements showed similar values for the cases of large gas flow rates. It is difficult to resolve single bubbles in this flow regime. When the number of bubbles in the liquid becomes less at low gas flow rates, the chance of capturing no bubble region will increase for the fast X-ray CT, resulting in small values of average void fraction. In this sense, the wire-mesh sensor with high sampling frequency is suitable for bubbly flow of low void fraction. Fig. 11 shows the comparison of the average void fraction obtained from the wire-mesh sensor and the fast X-ray CT for bubbly and slug flows. A tendency is observed that the fast X-ray CT under estimates the void fraction especially in bubbly flow regime. To improve the measurement quality for the fast X-ray CT, the following measures are undertaken: 1) adaptive selection of threshold for binarization, 2) development of detector with large-size pixels, and 3) development of X-ray sources of uniform intensity.

6 Conclusion

Concept and operation of a fast X-ray CT scanner were described in detail. A highly sensitive X-ray semi-conductor detector was newly developed and installed to increase the detection capability of the system. After the temporal and spatial resolutions were examined by both simulations and the phantom tests, the system was applied to air-water two-phase flow. Detailed dynamic interface was successfully visualized by the system.

To verify the interface measurements, the wire-mesh sensor was installed close to the measurement plane of the fast X-ray CT. The same two-phase flows were simultaneously measured by the both systems and their results were compared to each other. Comparison of the time series of the cross section averaged void fraction from both systems showed sufficient agreement for slug flow at large void fractions, while the fast CT underestimated the void fraction of bubbly flow especially in low void fraction range. Further hardware improvement is in progress to achieve better resolution with the fast X-ray CT scanner.

Acknowledgement

A part of this study was financially supported by the Budget for Nuclear Research of the Ministry of Education, Culture, Sports, Science and Technology, Based on the screening and counseling by the Atomic Energy Commission. Also, a part of this study has been performed as a public subscription project of practical and innovative nuclear power development by Institute of Advanced Energy (IAE) and Japan's Ministry of Economics, Trade and Industry (METI).

(Received on 18 February 2003)

Nomenclature

Sign	unit	Denomination
α	–	void fraction
a_i	1/m	Interfacial area concentration
A_p	m^2	cross section area of a pipe
A_{bi}	m^2	cross section area of a bubble
L_{ai}	m	Interface length of a bubble
dz	m	slice thickness
x, y, z	m	co-ordinates
j_g	m/s	gas superficial velocity
j_l	m/s	liquid superficial velocity

References

1 *Bord, S.; Clement, A.; Leconte, J. C.; Marmeggi, J. C.:* An X-ray tomography facility for I.C. industry at STMicroElinzugelectronics Grenoble. J. Microelectronics Engineering 1 (2002)
2 *Grodrian, S.; Schnopfer, S.:* Digital computed laminography and tomosynthesis - functional principles and industrial applications. Proc. Computerized Tomography for Industrial Applications and Image Processing in Radiology, March 15–17, Berlin, Germany, 1999
3 *Morooka, S.; Ichizuka, T.; Iizuka, M.; Yoshimura, K.:* Experimental study on void fraction in a simulated BWR Fuel Assembly (Evaluation of Cross-sectional averaged void fraction). Nuclear Engineering and Design 114 (1989) 91
4 *Matsubara, T.; Morooka, S.; Sakaki, K.; Tsuroyama, S.; Yoshimura, K.:* Void Fraction Within Rod Bundles Based on Three-fluid Model and Comparison with X-ray CT Void Data. Nuclear Engineering and Design 120 (1990) 203
5 *Tiseanu, I. and Simon, M.:* High-resolution cone-beam tomography for two-phase flow diagnostics. Proc. of 2nd International Symposium on Two-Phase Flow Modelling and Experimentation, May 23–26, Pisa, Italy, 1999
6 *Kumar, B. S.; Moslehian, D.; Dudukovic, M. P.:* A Gamma Ray Tomographic Scanner for Imaging Void Fraction Distribution in Bubble Columns. Flow Meas. Instru.6 (1995) 61
7 *Hori, K. and Akai, M.:* Measurement of Variation in Void Fraction Distribution by the Fast X-ray CT Scanner. Graphic Simulation and Visualization of Multiphase Flow 21 (1993) 96
8 *Hori, K.; Fujimoto, T.; Kawanishi, K.:* Application of cadmium telluride detector to high speed X-ray CT scanner. Nucl. Instr. and Methods in Physics Research A 380 (1996) 597
9 *M. Misawa, K.; Ichikawa, N.; Akai, M.; Hori, K.; Tsutsui, K.; Matsui, G.:* Development of Fast X-ray CT System for Transient Two-Phase Flow Measurement. Proc. 6th Int. Conf. Nucl. Eng., ICONE-6383, San Diego, USA, 1998
10 *Prasser, H.-M.; Scholz, D.; Zippe, C.:* Bubble size measurement using wire-mesh sensors. Flow Measurement and Instrumentation 12 (2001) 299

The authors of this contribution

Dr. *Masaki Misawa*, Dr. *Naoki Ichikawa*, *Makoto Akai*, National Institute of Advanced Industrial Science and Technology, 1–2–1 Namiki, Tsukuba, Ibaraki, 305–8564, Japan, e-mail: m.misawa@aist.go.jp
Dr. *Ion Tiseanu*, Institute of Atomic Physics, INFLPR Laboratory 22, PO Box MG-36, Bucharest-Magurele, R-76900, Romania, e-mail: tiseanu@alpha2.infim.ro
Dr. *Horst-Michael Prasser*, Forschungszentrum Rossendorf e. V., P.O. Box 510119, D-01314 Dresden, Germany, e-mail: prasser@fz-rossendorf.de